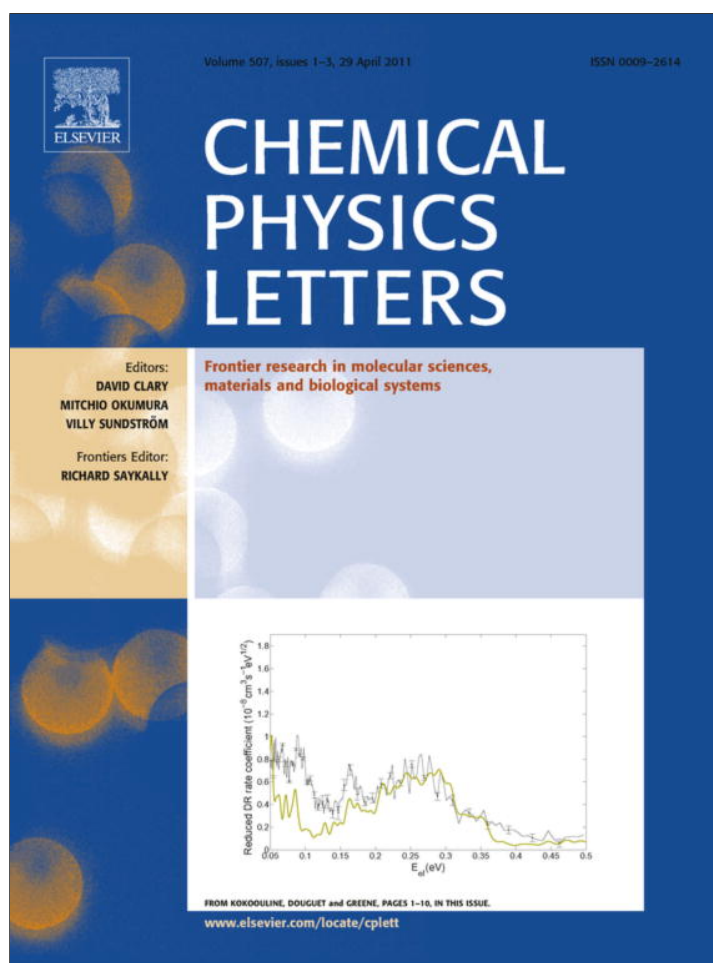


Provided for non-commercial research and education use.  
Not for reproduction, distribution or commercial use.



This article appeared in a journal published by Elsevier. The attached copy is furnished to the author for internal non-commercial research and education use, including for instruction at the authors institution and sharing with colleagues.

Other uses, including reproduction and distribution, or selling or licensing copies, or posting to personal, institutional or third party websites are prohibited.

In most cases authors are permitted to post their version of the article (e.g. in Word or Tex form) to their personal website or institutional repository. Authors requiring further information regarding Elsevier's archiving and manuscript policies are encouraged to visit:

<http://www.elsevier.com/copyright>



Contents lists available at ScienceDirect

## Chemical Physics Letters

journal homepage: [www.elsevier.com/locate/cplett](http://www.elsevier.com/locate/cplett)

## Measurement of vapor pressures using X-ray induced fluorescence

J.J. Curry<sup>a,\*</sup>, E.G. Estupiñán<sup>b</sup>, A. Henins<sup>a</sup>, W.P. Lapatovich<sup>b,1</sup>, S.D. Shastri<sup>c</sup><sup>a</sup> National Institute of Standards and Technology, Gaithersburg, MD, United States<sup>b</sup> OSRAM SYLVANIA, Inc., Beverly, MA, United States<sup>c</sup> Advanced Photon Source, Argonne National Laboratory, Argonne, IL, United States

## ARTICLE INFO

## Article history:

Received 22 November 2010

In final form 18 March 2011

Available online 22 March 2011

## ABSTRACT

X-ray induced fluorescence is demonstrated as a novel and fast method for measuring vapor pressures at high temperatures and high pressures. As such, it is an excellent complement to the effusion method, which is limited to lower pressures. High-energy synchrotron radiation was used to measure the total densities of Dy in the equilibrium vapor over condensed DyI<sub>3</sub> and Tm in the equilibrium vapor over condensed TmI<sub>3</sub>. Corresponding vapor pressures were determined with measured vapor cell temperatures across a range of vapor pressures of nearly three orders of magnitude, from less than 10<sup>2</sup> Pa to more than 10<sup>4</sup> Pa. Individual data points were obtained in time periods ranging from 10 to 30 s each.

Published by Elsevier B.V.

## 1. Introduction

Vapor pressures in equilibrium with solid or liquid materials are indicative of fundamental thermodynamic parameters such as enthalpies, entropies, and free energies of formation. Knowledge of vapor pressure curves are essential to many industrial processes and commercial technologies. Among these are metal–halide high-intensity discharge (HID) lamps in which the vapor pressures of metal atoms in the discharge are a determining factor in color-rendering and luminous efficacy. Accurate knowledge of vapor pressures in equilibrium with complex metal–halide mixtures is essential to the design of new lamps.

A commonly used method for determining vapor pressures is the effusion technique, of which there are many variants [1]. The basic method involves the effusion of mass from a Knudsen cell and the measurement of mass loss per unit time, either through direct mass measurements or through the measurement of torque on a torsion apparatus. To ensure that transport from the cell is in the effusion regime, the mean free path of escaping molecules must be much larger than the diameter of the effusion aperture. This limits the maximum pressure at which the effusion method is useful to the order of 100 Pa. Combining mass spectroscopy with effusion from a Knudsen cell makes it possible to infer relative densities of various molecular species in the vapor (see, for example, [2–4]).

As part of our study of metal–halide salts used in HID lamps, the limitations of the effusion method motivated us to search for an alternative method of measuring vapor pressures. The pressure ranges of greatest interest for lamp applications are above 100 Pa and we required the ability to survey a large range of temperatures

for a large number of metal–halide systems in a relatively short time. X-ray induced fluorescence (XRIF) suggested itself because of our earlier use of this technique as a plasma diagnostic in operating HID lamps [5]. There, XRIF was used to measure spatial distributions of a variety of elements, which were not necessarily in equilibrium with a solid or liquid phase. Of primary interest were density ratios and their spatial variations as the result of plasma effects. Here, we focus for the first time on the use of XRIF for the determination of vapor pressures in full equilibrium with a solid or liquid condensate.

XRIF, as used here, directly measures the total number density of atoms  $n$  of a particular atomic number  $Z$ ,

$$n_Z = \sum_i c_{Zi} M_i, \quad (1)$$

summed over all  $i$  molecular species  $M$  that contain  $c > 0$  atoms with atomic number  $Z$ . We refer to the densities  $n_Z$  as total densities of element  $Z$  or sometimes as elemental densities. In the past, the atomic number  $Z$  has been replaced by the corresponding chemical symbol.

Vapor pressures corresponding to the total densities of element  $Z$  can be defined as

$$p_Z = n_Z kT = kT \sum_i c_{Zi} M_i, \quad (2)$$

where  $k$  is Boltzmann's constant and  $T$  is the measured temperature of the vapor cell in equilibrium. The parameter  $p_Z$  will be referred to as the vapor pressure corresponding to the total density of element  $Z$ . This pressure differs from a sum of partial pressures when  $c_{Zi} > 1$  for any  $i$ . In many cases, the maximum value of  $i$  will be only 1 or 2.

XRIF does not, in the general case, allow us to directly determine the partial pressures of each molecular species in the gas phase. Although it does determine elemental content of the vapor,

\* Corresponding author.

E-mail address: [jjcurry@nist.gov](mailto:jjcurry@nist.gov) (J.J. Curry).<sup>1</sup> Present address: 51 Pye Brook Lane, Boxford, MA 01921, United States.

and thus puts constraints on the molecular densities, it is not an alternative to gas phase analysis by mass spectroscopy. XRIF is an alternative to mass-loss or torsion methods, which also do not determine partial pressures.

XRIF is not as well suited for the measurement of lighter elements (low  $Z$ ), since the characteristic X-ray fluorescence of the element must be energetic enough to escape the vapor cell being used. We used polycrystalline alumina (PCA) to construct our vapor cells because of its ability to withstand high temperatures and chemically-reactive species. The most prominent K-shell fluorescence line for any element is the  $K\alpha_1$  line. In ruthenium, the energy of this line is 19279 eV; for iodine it is 28612 eV; and for samarium it is 40118 eV. These lines have transmissions through 1 mm of PCA of 0.37, 0.71, and 0.85, respectively. As these examples show, fluorescence energy and fluorescence transmission increase with increasing atomic number. For a given experiment, lighter elements are more difficult to observe.

In this Letter, we demonstrate the applicability of XRIF to the determination of vapor pressures. We have measured the total density of Dy in the equilibrium vapor over both solid and liquid  $DyI_3$  and the total density of Tm in the equilibrium vapor over both solid and liquid  $TmI_3$ . The vapor pressures corresponding to these total densities range from a few tens of Pa near 1050 K to almost  $10^5$  Pa at temperatures approaching 1400 K. These measurements were obtained, along with many other similar measurements, during a 96 h period at the Advanced Photon Source, Argonne National Laboratory. We believe the XRIF technique will enable a substantial increase in the quantity and quality of vapor pressure measurements, particularly for vapor pressures greater than 100 Pa.

The significance of this application of XRIF lies in its speed and applicable pressure range as compared to effusion methods.

## 2. Method

The general technique of XRIF is described in Ref. [5] and fundamental concepts can be found in Ref. [6].

Figure 1 shows the arrangement of the experimental apparatus. The measurements were made on the 1-ID Beamline at the Advanced Photon Source [7]. Beamline optics [8] produce a monochromatic beam of X-rays whose energy can be tuned continuously over the range 40–130 keV. We used an unfocused

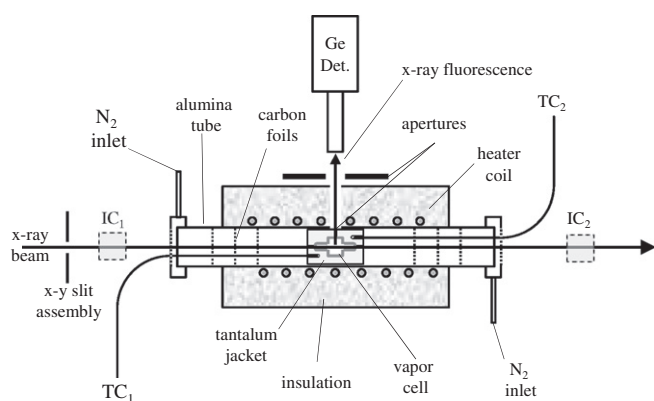


**Figure 1.** Schematic (top-view) of the experiment used to determine vapor pressures with X-ray induced fluorescence. IC<sub>1</sub> and IC<sub>2</sub> are ion chambers that measured the X-ray flux before and after the oven that contained the polycrystalline alumina vapor cell. Fluorescence induced in the vapor by the X-ray beam is emitted isotropically, but observed by the germanium detector (Ge Det.) only in the solid angle defined by the apertures. Thermocouples TC<sub>1</sub> and TC<sub>2</sub> measured the temperature of the tantalum jacket surrounding the vapor cell. Oxidation of the tantalum was prevented by a small flow of dry nitrogen driven by a slight over-pressurization at the N<sub>2</sub> inlets. The figure is not to scale.

beam whose photon flux was of order  $10^{12} \text{ s}^{-1}$  in a  $1 \text{ mm} \times 1 \text{ mm}$  cross section. Beam divergence was less than  $20 \mu\text{rad}$  in both the horizontal and vertical directions.

The monochromatic X-ray beam entered from the left and passed through a beam defining slit assembly, an ionization chamber, the oven containing the measurement cell, and finally another ionization chamber. The slit assembly was used to trim the beam size to  $500 \mu\text{m} \times 500 \mu\text{m}$ , with a proportional decrease in the photon flux, so that it would pass through the small X-ray windows and apertures in the oven with minimal scattering. The ionization chambers monitored the incident flux  $\Phi_i$  and transmitted flux. Characteristic X-ray fluorescence excited in the vapor by the incident X-rays was viewed along a direction perpendicular to the incident beam by an energy-resolving germanium crystal detector. The detector has an energy resolution of a few hundred eV. The field of view of the detector was limited by a small aperture in the oven and by an external aperture in order to reduce the detection of X-rays scattered from the cell relative to fluorescence X-rays from the vapor.

The central component of the oven is a 2.8 cm inner diameter by 31 cm long alumina tube spiral-wrapped with a heater wire. Around the section of the tube covered by the heater coil is an insulating layer of fused silica wool surrounded by a stainless steel shell. The ends of the alumina tube are covered by aluminum caps, each of which has a small graphite foil X-ray window, a hole for a thermocouple feed, and an inlet for dry nitrogen. The latter were used to purge the oven of oxygen before and during heating. Additional graphite foils between the end caps and the center of the oven limited convective heat loss along the tube. The oven was powered by a 300 V, 5 A solid-state direct-current power supply.

The vapor cell was held in the center of the oven by a cylindrical two-piece tantalum jacket that fits together closely around each cell. A close-up view is shown in Figure 2. (The alumina tube diameter was increased during construction to accommodate a sealed filling stem on the vapor cell. The additional room between the tantalum jacket and the alumina tube was filled with a carbon spacer, which is not shown in order to maintain the clarity of the figure.) The tantalum jacket has two 1.6 mm diameter holes that allowed the incident X-ray beam to enter and exit the cell. A third hole, measuring 1.3 mm in diameter by 3.6 mm long, allowed the induced fluorescence to escape in the direction of the detector. Tantalum was used because it combines a high heat conductivity

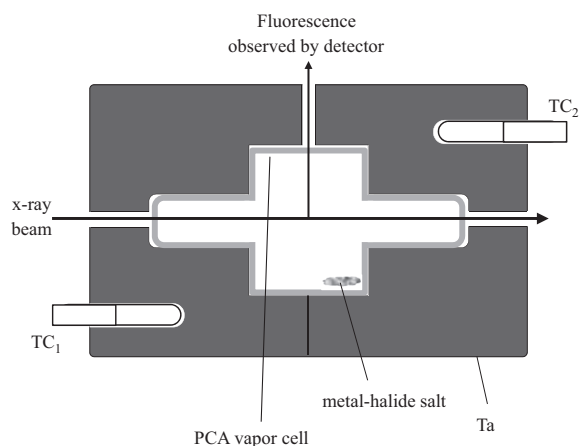


**Figure 2.** Detail of the PCA vapor cell and surrounding tantalum jacket. TC<sub>1</sub> and TC<sub>2</sub> are thermocouples that measured the temperature of the jacket. X-ray fluorescence was induced all along the beam in the vapor cell, but only the region in the center of the cell was observed by the detector. Except for the thermocouples and the hole through which the fluorescence was observed, the jacket and cell are cylindrically symmetric. The vapor cell length is nominally 25 mm.

with high X-ray opacity. High heat conductivity reduces temperature variations across the cell, while X-ray opacity defines the beam position and limits X-ray scattering into the detector. The side hole in the tantalum was a limiting aperture for the field of view of the detector. The temperature of the tantalum was measured by a pair of type-N thermocouples, one deeply embedded in each half of the tantalum jacket. The voltage induced across each thermocouple was read by a digital multimeter and converted to a temperature by use of a standard temperature table. The ambient temperature near the junction between the thermocouples and multimeters was also monitored to provide a reference temperature.

Each vapor cell is made of PCA, a materials choice determined by the requirements of a hermetically-sealed cell, X-ray access to the contained vapor, and minimization of reactions with the vapor. Tantalum has been used in many previous studies of rare earth-halide vapors because of its reputed low reactivity with these salts, but it does present difficulties with the other two requirements. Some reactivity between rare earth-halide salts and PCA is known from a great deal of practical experience with much harsher conditions in commercial metal-halide lamps, but it is rather slow and is not detrimental to lamp operation during the first few thousand hours of operation. Our measurements were made in cells with less than 100 h at elevated temperatures.

The PCA cells are 25 mm long with a typical wall thickness of 0.8 mm, cylindrically-symmetric, and shaped to reduce Compton scattering of beam photons into the detector (Figure 2). Compton scattering changes both the direction and energy of a photon, sometimes causing overlap with fluorescence lines in observed spectra. The tantalum jacket prevented photons scattered from points where the beam entered and exited the cell from directly entering the detector (first-order scattering). The shape of the cell and the close-fitting tantalum jacket prevented second-order scattering that occurs when photons scattered at the beam entrance and exit points reach the detector by scattering a second time from parts of the cell that are in the field-of-view of the detector. Thus a beam photon must be scattered at least three times from the cell in order to enter the detector. Scattering from the vapor is considerably less likely than scattering from the cell because the vapor density is several orders of magnitude lower than the PCA density. In addition, first-order scattering from the vapor was nearly eliminated by choosing the detector axis to coincide with the direction of polarization of the beam X-rays [6,9].

The number of XRIF photons,  $C$ , in a  $K_{\eta}$  spectral line at energy  $E_{K\eta}$  recorded by the detector is [5]

$$C_Z(E_{K\eta}) = \Phi_i \sigma_Z^K(E_i) Y_Z^K B_Z^K \frac{\Omega}{4\pi} VT(E_i) T(E_{K\eta}) Q_d(E_{K\eta}) n_Z, \quad (3)$$

where  $\Phi_i$  is the incident photon flux per unit time,  $\sigma_Z^K(E_i)$  is the  $K$ -shell photoelectric absorption cross-section for the element of atomic number  $Z$  at the beam photon energy  $E_i$ ,  $Y^K$  is the  $K$ -shell fluorescence yield,  $B$  is the branching fraction for the line being observed,  $\Omega$  is the solid angle subtended by the detector,  $V$  is the volume common to both the field of view of the detector and the X-ray beam,  $T(E_i)$  is the transmission of incident photons from the point of flux measurement to the point of observation,  $T(E_{K\eta})$  is the transmission of fluorescence photons from the point of observation to the detector,  $Q_d$  is the detector efficiency, and  $n_Z$  is the observed gas phase number density. The atomic parameters can be obtained from a variety of widely available compilations. The transmission factors can be easily calculated from such data sources.  $\Phi_i$  was measured during the experiment and the geometric factors  $\frac{\Omega}{4\pi} V$  were obtained by observing fluorescence from an identical vapor cell containing a known density of Xe. Our detector response is flat over the range 19–70 keV.

### 3. Our measurements

We prepared several vapor cells, each dosed with a few mg of the desired salt and 700 Pa of Ar. Several additional cells were dosed only with various pressures of Xe ranging from 100 to  $10^3$  Pa. The latter were used to obtain the absolute calibration of the vapor pressure measurements by comparison.

We made measurements with beam energies of 61 and 86 keV. The lower beam energy provided larger fluorescence signals because absorption cross sections increase with decreasing energy except at excitation thresholds. The higher beam energy allowed us to check for the presence of vapor contaminants as heavy as thallium because excitation thresholds increase with atomic number. None were found.

The tantalum jacket and vapor cell equilibrate with a time constant of tens of seconds, while the oven has a time constant in the range of 20 min. Thus we found it preferable, because of time constraints, to allow the temperature of the oven to drift upward at a rate slow enough for the vapor cell to sufficiently equilibrate with the tantalum jacket. The sufficiency of the equilibration was tested by comparing values obtained during a slow warm-up with values obtained during a much more rapid cool-down. Increasing the rate of temperature change by more than an order of magnitude changed the pressure measurement by less than 10%. We conclude that our typical rate of change of 0.02 K/s was slow enough for the vapor cell to equilibrate at a temperature within a few degrees of the temperatures measured by the thermocouples. The acquisition of each data point was fast enough (10–30 s) that the maximum temperature change during any measurement was 1.5 K, with the typical change less than 1 K.

A typical fluorescence spectrum is shown in Figure 3 for the case of  $\text{TmI}_3$  at  $T = 1175$  K. The total densities of Tm and I were determined by integrating the respective  $K\alpha$  peaks. The low, wide background starting at 45 keV and extending to higher energies is mostly due to Compton scattering of beam photons. The background under each fluorescence peak was estimated by a fitting procedure on both sides of the peak.

### 4. Results and discussion

The vapor pressures corresponding to our measurements of the total densities of Dy and Tm are given in Figures 4 and 5, respectively, where the customary  $\log_{10} p$  is plotted versus  $1/T$ . Statistical uncertainties arising from limited photon counts in the spectral lines and random background counts are indicated by vertical bars for representative data points. Uncertainties range from 40% at the

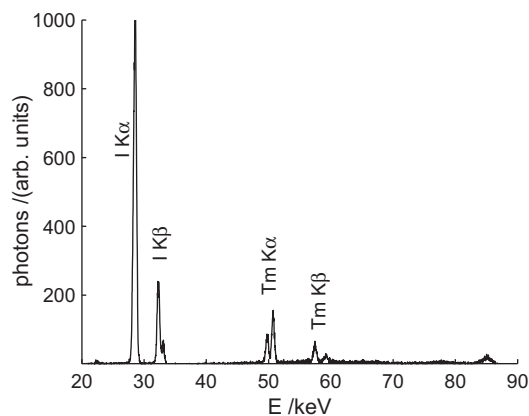
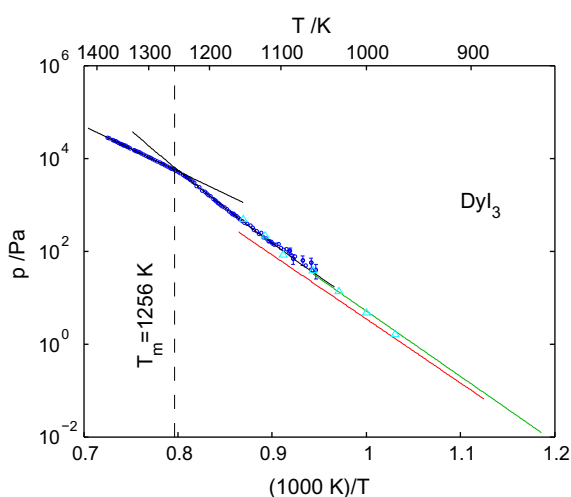
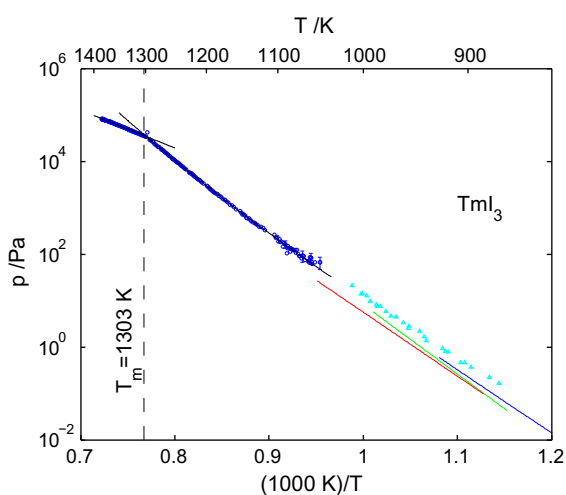


Figure 3. X-ray induced fluorescence spectrum acquired from a vapor cell containing  $\text{TmI}_3$  at 1175 K.



**Figure 4.** Vapor pressure corresponding to the total density of Dy over condensed  $\text{DyI}_3$ , and other measurements, as a function of temperature: blue circles, this work; green line, Hirayama et al. [4]; red line, Brunetti et al. [11]; cyan triangles, Kaposi et al. [3]. Solid black lines are weighted least-squares fits of Eq. (4) to the data below  $T = 1230$  K and Eq. (5) to data above 1255 K. The fitting coefficients are given in Table 1. The dashed vertical line shows the tabulated melting point of  $\text{DyI}_3$  [10].



**Figure 5.** Vapor pressure corresponding to the total density of Tm over condensed  $\text{TmI}_3$ , and other measurements, as a function of temperature: blue circles, this work; green line, Hirayama et al. [4]; red line, Brunetti et al. [14]; cyan triangles, Dettingmeijer et al. [2]; blue line, Karwath et al. [13]. Solid black lines are weighted least-squares fits of Eq. (4) to the data below  $T = 1294$  K and Eq. (5) to data above 1300 K. The fitting coefficients are given in Table 1. The dashed vertical line shows the tabulating melting point of  $\text{TmI}_3$  [10].

lowest vapor pressures to less than 0.5% at the highest pressures, with the latter being imperceptible on the scale of the graphs. Measurements were made at temperatures lower than shown, but had uncertainties greater than  $\pm 40\%$ . Melting points for the pure salts [10] are indicated by dashed vertical lines.

Measurements of vapor pressures over condensed  $\text{DyI}_3$  have also been reported by Hirayama et al. [4], Kaposi et al. [3], Brunetti et al. [11], and Hilpert et al. [12]. Hirayama et al. [4] measured mass-loss by effusion from a Knudsen cell over the temperature range 843–1060 K. Their results were calibrated by comparison with the well-known vapor pressure of zinc. Brunetti et al. [11] measured the torsion on an effusion cell over the temperature

range 889–1157 K. Absolute vapor pressures were determined by comparison with the well-known vapor pressures of Cd and Pb, with estimated uncertainties in the range of 15–25%. Kaposi et al. [3] derived absolute vapor pressures from ion currents measured by mass spectrometer over the temperature range 970–1150 K. Hilpert et al. [12] scaled their results with those of Hirayama et al. [4], so their absolute values cannot be considered independent.

Both Hirayama et al. [4] and Brunetti et al. [11] assumed a vapor consisting only of monomers  $\text{DyI}_3$  and summarized their results with analytic expressions that appear in Figure 4 and Table 1. The results of Kaposi et al. [3] and of Hilpert et al. [12] indicate a small, but finite, presence of dimers  $\text{Dy}_2\text{I}_6$ . Hilpert et al. [12] obtained a dimer partial pressure of 12% of the total pressure at 1050 K, but Kaposi et al. [3] found a value four times lower. In both cases the dimer fraction increased with temperature. For Kaposi et al. [3], we have plotted  $p_{\text{mono}} + 2p_{\text{dimer}}$  using their reported partial pressures for the monomer and the dimer in order to obtain a more direct comparison to our own results.

Measurements of vapor pressures over condensed  $\text{TmI}_3$  have been reported by Hirayama et al. [4], Dettingmeijer et al. [2], Karwath et al. [13], and Brunetti et al. [14]. Hirayama et al. [4] made measurements of  $\text{TmI}_3$  at the same time they studied  $\text{DyI}_3$ . Using the same methods, they covered the temperature range 867–990 K. Dettingmeijer et al. [2] measured mass-loss from a Knudsen effusion cell, calibrated by comparison with the well-known vapor pressure of zinc, over the temperature range 874–1032 K. In addition, Dettingmeijer et al. [2] performed mass spectral analysis of the vapor and reported partial pressures for both the monomer and dimer. Karwath et al. [13] measured mass-loss and mass spectra from a Knudsen effusion cell and also reported partial pressures for both monomer and dimer. Brunetti et al. [14] made both mass-loss and torsion measurements for  $\text{TmI}_3$  over the temperature range 887–1051 K.

Again, Hirayama et al. [4] and Brunetti et al. [14] assumed the vapor over condensed  $\text{TmI}_3$  contained only  $\text{TmI}_3$  molecules, and the analytic expressions each group developed for the total vapor pressure are given in Figure 5 and Table 1. Dettingmeijer et al. [2] indicated that 25% of the total pressure at 900 K is due to the dimer, with the percentage increasing with temperature. On the other hand, Karwath et al. [13] report only 10% of the total vapor pressure at that temperature is from the dimer. For both Dettingmeijer et al. [2] and Karwath et al. [13], we have plotted  $p_{\text{mono}} + 2p_{\text{dimer}}$  using their reported partial pressures for the monomer and the dimer in order to obtain a more direct comparison to our own results.

We also attempted to fit our data with simple analytic expressions and found that the data below the melting points were best fit with the expression

**Table 1**  
Analytic expressions for measured vapor pressures.

Salt	T (K)	$\log_{10}(p)$ (Pa)	Source
$\text{DyI}_3$	1056–1229	$-91.4(\pm 0.5) + 30.7(\pm 0.16) \log_{10}(T/\text{K})$	This work <sup>a</sup>
	1255–1379	$11.492(\pm 0.014) - 9700(\pm 200)/(\text{K}/T)$	This work <sup>a</sup>
	843–1060	$14.80(\pm 0.14) - 14090(\pm 133)/(\text{K}/T)$	[4] <sup>b</sup>
	889–1157	$14.34(\pm 0.20) - 13800(\pm 200)/(\text{K}/T)$	[11] <sup>b</sup>
$\text{TmI}_3$	1048–1294	$-90.88(\pm 0.11) - 30.64(\pm 0.04) \log_{10}(T/\text{K})$	This work <sup>a</sup>
	1300–1384	$10.785(\pm 0.010) - 8123(\pm 13)/(\text{K}/T)$	This work <sup>a</sup>
	867–990	$15.9(\pm 0.2) - 14950(\pm 190)/(\text{K}/T)$	[4] <sup>b</sup>
	781–925	$\log_{10}(10^{13.7-13000/T} + 2 \times 10^{16.71-16500/T})$	[13] <sup>a</sup>
	887–1051	$14.54(\pm 0.20) - 13800(\pm 200)/(\text{K}/T)$	[14] <sup>b</sup>

<sup>a</sup> Vapor pressure as defined by Eq. (2).

<sup>b</sup> Assumes a monomer only.

$$\log_{10}P = A + B\log_{10}T, \quad (4)$$

while the data above the melting points were more closely fit by the expression

$$\log_{10}P = A + B/T. \quad (5)$$

Values of the fitting coefficients  $A$  and  $B$  are given in Table 1 along with similar analytic expressions for existing data. For Dy, our fitted curves intersect at 1245, 11 K lower than the tabulated melting point [10]. Solid-state phase transitions have been observed in  $\text{DyI}_3$  at 1101 K [15], 1135 K [16], and at 1244 K [17]. The latter is at essentially the same temperature where our curves intersect and only 12 K from the melting point. To what degree this transformation affects the vapor pressure curve is unknown. For Tm, our fitted curves intersect at 1300, 3 K less than the tabulated melting point [10].

Figures 4 and 5 emphasize the considerably higher pressures and temperatures for which the XRIF technique is useful compared to previously utilized methods.

The preliminary nature of this phase of the work has not given us the opportunity to fully understand the sources and magnitudes of systematic errors associated with this technique. However, we can make some comments. Two possible sources of significant measurement error are: (1) the unknown difference between the measured temperature and the actual temperature of the salt and (2) the sensitivity of the calibration to changes in position of the vapor cell. The first of these arises because of spatial temperature variations between the thermocouple and the salt. The second arises because an aperture on the tantalum jacket is one of the limiting apertures for fluorescence collection and this aperture is not rigidly fixed relative to the second limiting aperture. Changes in its position change the fluorescence collection efficiency, or equivalently the  $\Omega V$  term in Eq. (3). Measurements of Xe over the range of temperatures from ambient to 1300 K show a linear change in the signal of 10%. Comparable errors may occur every time a new cell is put in the oven, including for calibrations. In the future, these issues will be addressed by dosing the cells with Xe instead of Ar so that each spectrum provides its own internal calibration. Errors in the nominal pressures in the Xe calibration cells are not well characterized yet.

At higher vapor pressures, absorption of both beam and fluorescence X-rays by the vapor becomes significant. Corrections for absorption of both the X-ray beam and the fluorescence by the vapor and by the cell walls have been made. Corrections as high as 25% have been made for attenuation by the walls. These corrections can be in error by as much as 10% of the correction value, or 2–3% of the data value, due to variations in the cell wall thickness or density. Corrections due to absorption by the vapor were at most 5% of the data value and were necessary only at the highest vapor pressures. At vapor pressures an order of magnitude larger than measured here, errors in the correction can become significant. A smaller cell and higher beam energy could partially mitigate such a problem.

The atomic parameters in Eq. (3) are generally known to within a few percent provided the energy is not coincident with the edge energy of one of the atomic shells. Branching ratios are likely the least accurately known atomic parameters, with errors being as high as 5%.

Although not reported here, our observed spectra also provided measurements of total I densities in the vapor. These

measurements show anomalously high I pressures, especially at temperatures too low for the rare-earth metals to be seen. Thermodynamic calculations suggest that this may be due in part to contamination of the salt with a small amount of water vapor. Although the I vapor pressure is strongly perturbed, the calculations show little effect on the rare-earth pressures. A more detailed discussion of the I pressures is beyond the scope of this Letter.

## 5. Conclusion

The measurements presented here demonstrate the capabilities of XRIF to obtain vapor pressures over a wide range of pressures and temperatures. The technique measures total elemental densities in the vapor from which corresponding vapor pressures are obtained using measured temperatures. Individual data points were acquired in tens of seconds, although at higher pressures, they could have been obtained in seconds. With better understanding and mitigation of systematic errors, we expect the technique to be capable of measurements with uncertainties as small as a few percent.

## Acknowledgments

We thank the management of OSRAM SYLVANIA for supporting this project and we thank Joanne Brown, Victor Perez, Jeff Neil, Michael Quilici, and John Kelso, all of OSRAM SYLVANIA, for their expert technical assistance. Use of the Advanced Photon Source at Argonne National Laboratory was supported by the US Department of Energy, Office of Science, Office of Basic Energy Sciences, under Contract No. DE-AC02-06CH11357.

## References

- [1] J.L. Margrave (Ed.), *The Characterization of High-Temperature Vapors*, John Wiley and Sons Inc., New York, 1967.
- [2] J.H. Dettingmeijer, H.R. Dielis, *J. Less-Common Metals* 139 (1988) 331.
- [3] O. Kaposi, L. Lelik, K. Balthazár, *High Temp. Sci.* 16 (1983) 299.
- [4] C. Hirayama, J.F. Rome, F.E. Camp, *J. Chem. Eng. Data* 20 (1975) 1.
- [5] J.J. Curry, H.G. Adler, W.K. Lee, S.D. Shastri, *J. Phys. D: Appl. Phys.* 36 (2003) 1529.
- [6] N.A. Dyson, *X-rays in Atomic and Nuclear Physics*, second ed., Cambridge University Press, Cambridge, 1990.
- [7] [www.aps.anl.gov/beamlines/directory/](http://www.aps.anl.gov/beamlines/directory/), 2010.
- [8] S.D. Shastri, K. Fezzaa, A. Mashayekhi, W.-K. Lee, P.B. Fernandez, P.L. Lee, *J. Synchrotron Rad.* 9 (2002) 317.
- [9] R.D. Evans, *Compton Effect in Encyclopedia of Physics*, vol. 34, Springer, Verlag, 1958, p. 218.
- [10] S. Hansen, R. Steward, J. Getchius, T. Brumleve, *Supplement to Vapor Pressure of Metal Bromides and Iodides*, APL Engineered Materials, Inc., Urbana, Illinois, 2000.
- [11] B. Brunetti, P. Vassallo, V. Piacente, P. Scardala, *J. Chem. Eng. Data* 44 (1999) 509.
- [12] K. Hilpert, M. Miller, F. Ramondo, *Thermochim. Acta* 417 (2004) 163.
- [13] T. Karwath, D. Kobertz, K. Hilpert, in: H. Wendt (Ed.), *Molten Salt Chemistry and Technology*, vol. 5, Trans Tech Publication, Ltd., Switzerland, 1998, p. 223.
- [14] B. Brunetti, V. Piacente, P. Scardala, *J. Chem. Eng. Data* 49 (2004) 832.
- [15] D.A. Johnson, J.D. Corbett, in: *The Rare Earth Elements*, vol. Tome 1, International Colloquium of the National Centre for Scientific Research, No.180, Editions du Centre National Scientific Research, Paris, 1970, Paris-Grenoble, 5–10 May, 1969, p. 429.
- [16] A.K. Molodkin, A.G. Dudareva, *Russ. J. Inorgan. Chem.* 31 (1986) 1603.
- [17] D. Kobertz, K. Hilpert, S. Hansen, in: M. Haverlag, G.M.W. Kroesen, T. Taguchi (Eds.), *Proceedings of the 12th International Symposium on the Science and Technology of Light Sources and the 3rd International Conference on White LEDs and Solid State Lighting*, FAST-LS, Ltd., Sheffield, UK, Eindhoven, The Netherlands, 2010, p. 521.